catalysts

MDPI

Article

Facile Sonication Synthesis of WS_2 Quantum Dots for Photoelectrochemical Performance

Liyan Zhou [1], Shancheng Yan [2,*], Han Wu [1], Haizeng Song [2] and Yi Shi [1,*]

[1] National Laboratory of Solid State Microstructures, School of Electronic Science and Engineering, Nanjing University, Nanjing 210093, China; njuzly@163.com (L.Z.); wuhan1106@yeah.net (H.W.)

[2] School of Geography and Biological Information, Nanjing University of Posts and Telecommunications, Nanjing 210023, China; songhaizeng0501@foxmail.com

* Correspondence: yansc@njupt.edu.cn (S.Y.); yshi@nju.edu.cn (Y.S.); Tel.: +86-25-85866634 (S.Y.); +86-25-83621220 (Y.S.)

Academic Editors: Alain Roucoux and Audrey Denicourt
Received: 28 November 2016; Accepted: 30 December 2016; Published: 6 January 2017

Abstract: Two-dimensional transition metal dichalcogenides, such as tungsten disulfide (WS_2), have been actively studied as suitable candidates for photocatalysts due to their unique structural and electronic properties. The presence of active sites at the edges and the higher specific surface area of these materials are crucial to the photocatalytic activity of the hydrogen evolution reaction. Here, WS_2 quantum dots (QDs) have been successfully synthesized by using a combination of grinding and sonication techniques. The morphology of the QDs was observed, using transmission electron microscopy and an atomic force microscope, to have uniform sizes of less than 5 nm. Photoelectrochemical (PEC) measurements show that the current density of WS_2 QDs under illumination is almost two times higher than that of pristine WS_2. Furthermore, these high-quality WS_2 QDs may have various applications in optoelectronics, solar cells, and biomedicine.

Keywords: tungsten disulfide; quantum dots; sonication; photocatalysis

1. Introduction

Photoelectrochemical (PEC) water splitting, which consumes continuous supplies and generates hydrogen, is considered to be an excellent engineering technique to obtain energy and solve environmental issues in the future. However, the scarcity and high cost of platinum severely limit the application of traditional high-performance platinum-based catalysts. New-generation materials with high photocatalytic activity and low cost have to be developed as alternatives. Since the discovery of graphene, 2D materials, such as tungsten disulfide (WS_2) and other transition metal dichalcogenides (TMDCs), have drawn a great deal of interest due to their attractive physical and electronic properties [1–3]. It is reported that the hydrogen binding energy of MoS_2 is close to that of Pt-group metals, thus hinting at potential applications of other TMDCs in photocatalytic HER [4–9]. Both computational and experimental results have confirmed that the photocatalytic activities of XS_2 (X could be other transition metals, such as W) mainly stem from the edges rather than the basal planes [10,11].

Quantum dots (QDs), with lateral sizes of less than 10 nm, usually exhibit unique electrical/optical behaviors from those of nanosheets or bulk materials [12,13]. Such QDs could provide abundant active edges and large specific surface areas, as well as quantum confinement, thus possibly promoting the photocatalytic activity. The layered structure of WS_2 is formed by unit S-W-S atomic trilayers through weak van der Waals interactions. Such a structure made it possible to obtain few-layer nanosheets and even QDs from the bulk form by exfoliation. Zhang et al. presented a combination of grinding and sonication techniques to prepare TMDC QDs from their bulk crystals [14]. Similar exfoliation

in aqueous solution instead of organic solvents has also been reported [15]. However, defect-free WS_2 has been difficult to obtain, and imperfections including sulfur vacancy defects and oxidized impurities may strongly affect the transport properties of the materials [16,17]. In our previous work, we have developed a facile low-temperature thiol chemistry route to repair the sulfur vacancies and improve the electrical properties [18–20]. Such a route may hinder the photo-generated electron-hole recombination and improve the photocatalytic activity.

In this work, WS_2 QDs were synthesized by a facile ultrasonication method from hydrothermal synthesized WS_2 powders, as shown in Figure 1. Further sulfuration was applied in order to reduce the amount of defects and improve the electrical properties of WS_2. Various characterizations confirmed the uniform morphology and properties of the quantum dots. Our results demonstrate that QDs with higher specific surface area and better electric conductivity can lead to better PEC activity for water splitting to produce hydrogen under visible light irradiation.

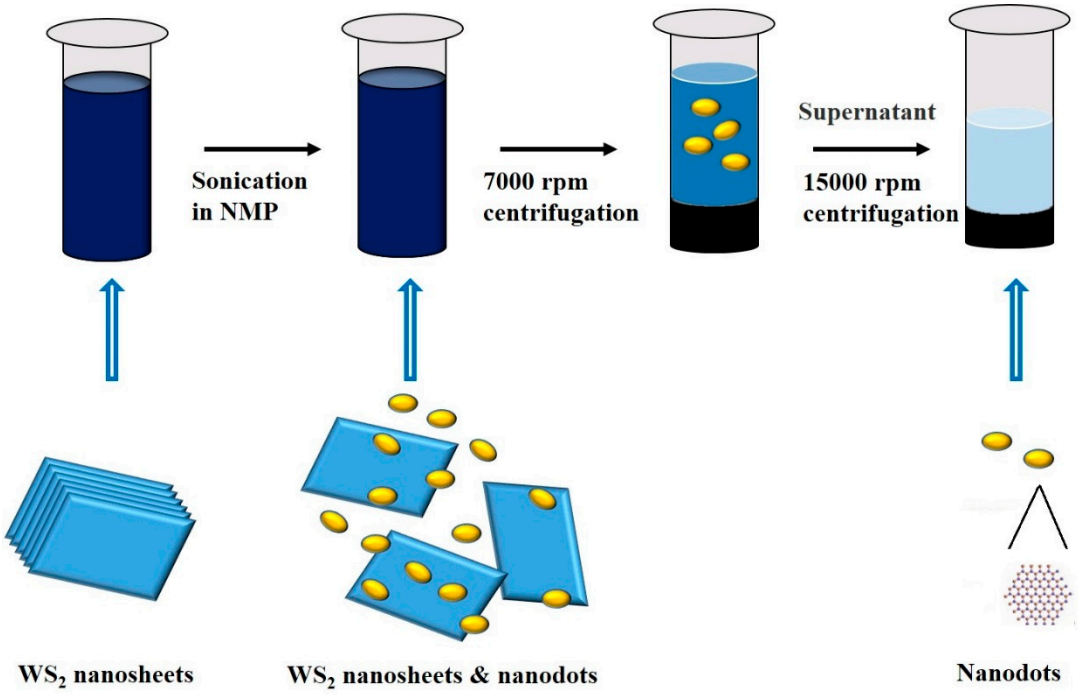

Figure 1. Synthesis process of WS_2 QDs (Quantum dots), including an ice-bath sonication and two-step centrifugation.

2. Results and Discussion

2.1. Morphology and Structure

Atomic force microscopy (AFM) and transmission electron microscopy (TEM) were used to measure the morphology of WS_2 QDs. Three QDs in nearly a straight line were characterized by AFM, as shown in Figure 2a,b. The heights of the QDs were mostly 2.5–4.0 nm, corresponding to three to five single layers of WS_2 [13,21]. Figure 2c shows a TEM image, showing uniform WS_2 QDs with an average size of ~3 nm. As shown in Figure 2d, a lattice spacing of about 0.21 nm can be indexed to (104) planes of the WS_2 crystal [21]. For comparison, the morphology of WS_2 consisting of large-scale and stacked layers was also characterized, as shown in Figure 2e,f. Such a small size of QDs could provide more active edges for photocatalytic activity.

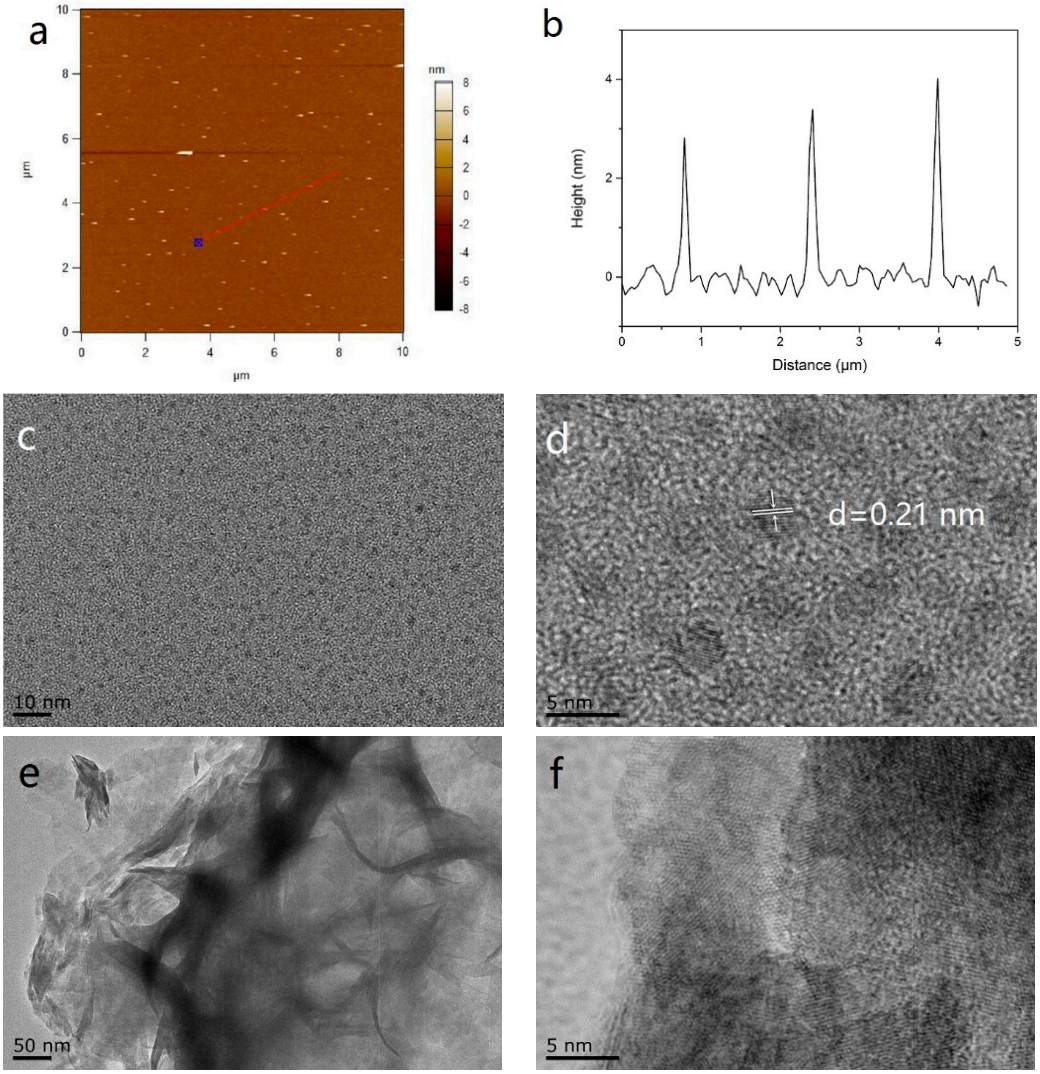

Figure 2. Morphology characterization of WS_2 QDs. (**a**) AFM (atomic force microscopy) image of WS_2 QDs; (**b**) Height profiles along the red line in (**a**); (**c**) TEM (transmission electron microscopy) and (**d**) HRTEM (high resolution transmission electron microscopy) image of WS_2 QDs; (**e**) TEM and (**f**) HRTEM image of hydrothermal synthesized WS_2.

2.2. X-ray Photoelectron Spectroscopy

XPS (X-ray photoelectron spectroscopy) spectra, shown in Figure 3, confirmed the chemical composition of the WS_2 QDs. Figure 3a shows the typical survey spectrum of WS_2 QDs. The full XPS spectrum of the products yielded an S/W ratio of 1.95, corresponding to the basis of WS_2. Here, the presence of C, W, S, and O was observed. The peaks of 4f-level W atoms that correspond to a +4 valence state bound (WS_2) are presented in Figure 3b. By multiple-peak separation, the bands at 31.7, 33.8 and 37.3 eV are assigned to W $4f_{7/2}$, W $4f_{5/2}$ and W $5p_{3/2}$, respectively. However, the band at 35.2 eV may be ascribed to the existence of residual WO_3. S peaks ($2p_{3/2}$ at ~161.2 eV and $2p_{1/2}$ at ~162.4 eV) in Figure 2c are attributed to the −2 valence state of S atoms. Our XPS results agree well with the reported values in our previous work [20,22], showing that QDs have the same chemical composition as the bulk materials.

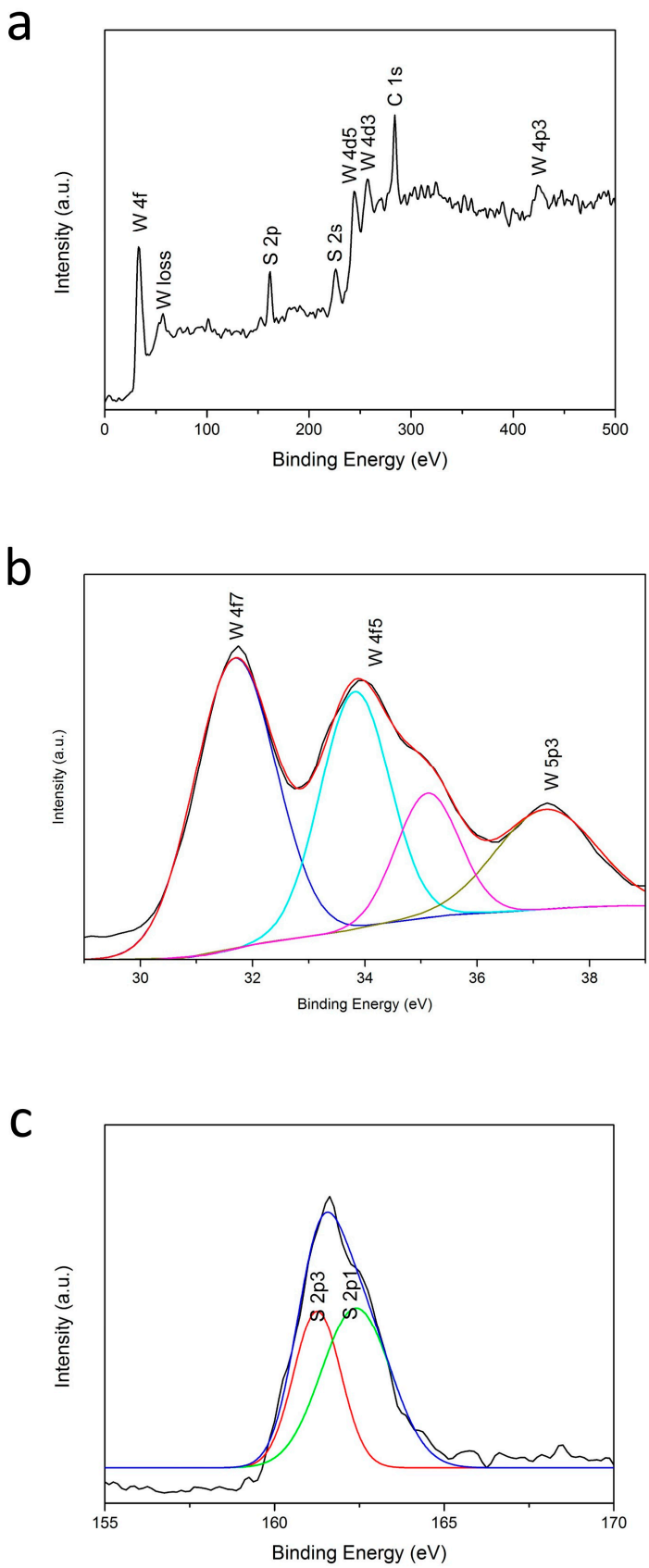

Figure 3. XPS spectra of WS_2 QDs. (**a**) Survey scan; (**b**) W4f; and (**c**) S2p peak, respectively.

2.3. Optical Properties

Raman and UV-vis (ultraviolet-visible) spectroscopy were carried out to identify the differences between the QDs and bulk materials. As shown in Figure 4a, the Raman peaks observed at 353 cm^{-1} and 418 cm^{-1} correspond to the E_{2g} and A_{1g} modes of WS_2, respectively [23–25]. There was almost no difference between the peak positions of the three samples. However, the peak intensity of QDs is obviously reduced. This may be caused by the absence of layer-layer interactions, with an increase of the dielectric screening which reduces the long-range Coulomb interaction between the effective charges and thus reduces the overall restoring force on the atoms [26,27]. Figure 4b shows the UV-vis spectrum of the original WS_2, sulfuration-treated WS_2 and treated WS_2 QDs. There was no obvious absorption peak for the original WS_2, which may be caused by defects. After sulfuration, distinct peaks can be observed at around 450 nm and assigned to the direct transition from the deep valence band to the conduction band. The peaks at around 660 nm can also be attributed to the K point of the Brillouin zone [28]. In terms of the QDs, the whole absorption spectrum was enhanced as compared with treated WS_2. This result reveals that the as-prepared WS_2 QDs may have better optical properties than the bulk materials.

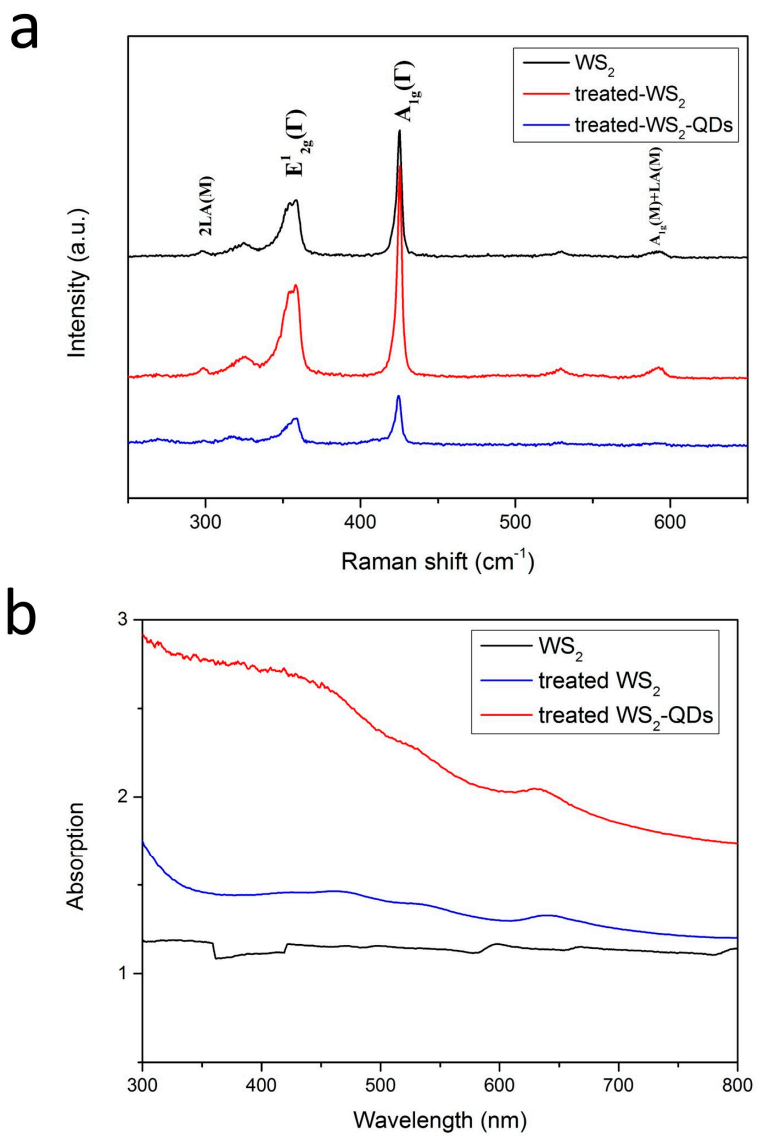

Figure 4. (**a**) Raman spectra and (**b**) UV-vis (ultraviolet-visible) spectra of WS_2, sulfuration-treated WS_2 and treated WS_2 QDs, respectively.

2.4. Photocatalytic Measurements

Based on the morphology and optical characterization, our samples were then explored as photocatalysts for HER. PEC activity was measured using a standard three-electrode electrochemical configuration combined with Xe illuminant (Figure 5a) in 0.5 M sodium sulfate (Na_2SO_4) solution with a scan rate of 10 mV/s [5,29]. As shown in Figure 5b, when the applied voltage was slowly increased from 0.2 V to −0.5 V, the empty ITO (Indium tin oxide) curve (green) was almost a straight line. All the WS_2, sulfuration-treated WS_2 and QD electrodes showed a cathodic current corresponding to the hydrogen evolution, while the current density of the QDs (blue curve) was enhanced more rapidly than that of bulk WS_2. These results may arise from two factors: (1) the WS_2 QDs have more active edge sites and surface area for PEC than the nanosheets or bulk materials; (2) the sulfuration processing has significantly removed the sulfur vacancies and improved the interface, consequently causing a better photoelectrochemical performance. Furthermore, under Xe-lamp illumination, the current density of WS_2 QDs (pink curve) was further increased. Under the same potential (−0.5 V Vs. Ag/AgCl), the current density of the WS_2 QDs under illumination was almost two times higher than that of the pristine WS_2. These benefits suggest good photocatalytic activities of WS_2 QDs.

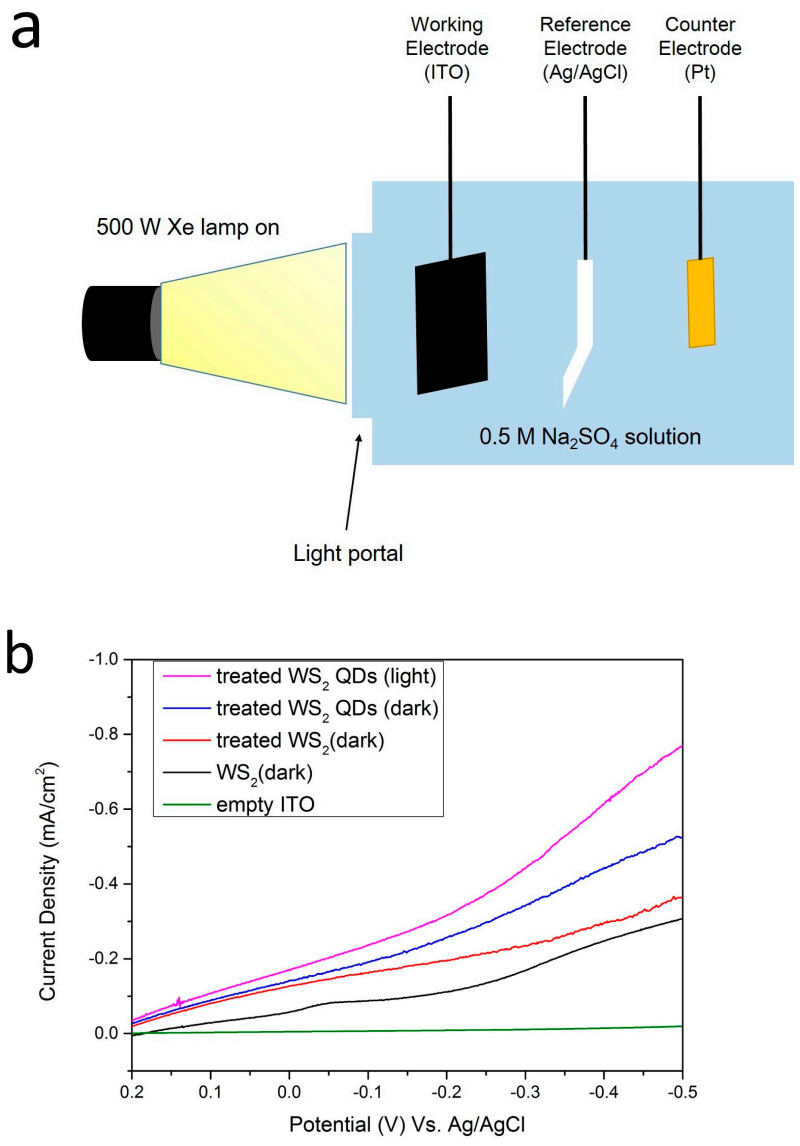

Figure 5. (**a**) Schematic diagram of photocatalytic measurement and (**b**) PEC (photoelectrochemical) activity of bulk WS_2, sulfuration-treated WS_2 and treated WS_2 QDs (dark and under light), respectively.

3. Materials and Methods

3.1. Synthesis

Tungsten hexachloride (WCl_6), thioacetamide (TAA) and (3-Mercaptopropyl) trimethoxysilane were purchased from Aladdin Industrial Corporation. All chemicals used are of analytical grade and applied as received without further purification.

In a typical experiment, WCl_6 (0.8923 g) and 1.6904 g of thioacetamide (TAA) were slowly added to DI (de-ionized) water (30 mL), stirred at room temperature for 1 h. The solution was then transferred into a reaction kettle and maintained at 265 °C for 24 h. After cooling to room temperature, the products were centrifuged and washed several times with DI water, and then dried in vacuum at 60 °C. For further sulfuration, initial WS_2 products were dispersed and dipped in a fresh solution of 1/15 (*v*/*v*) (3-Mercaptopropyl) trimethoxysilane/dichloromethane at 4 °C for 24 h. Both products were annealed at 300 °C for 3 h under Ar atmosphere.

WS_2 QDs were prepared by a facile ultrasonication method. Then 10 mg WS_2 (sulfuration-treated WS_2) powder and 20 mL NMP were put into a 20 mL bottle and sonicated for 6 h in an ice bath to exfoliate the WS_2 powder using a sonicator (KQ-3200E, Kunshan Ultrasonic Instruments Co. Ltd., Jiangsu, China) with an output power of 150 W. The suspensions were centrifuged for 20 min at 7000 rpm to separate the centrifugate and extract the supernatant. The respective batches of supernatant were then centrifuged for 40 min at 12,000 rpm and the centrifugate was further separated. The corresponding batches of precipitates were then extracted, washed and dissolved in ethanol.

3.2. Characterization

Atomic force microscopy (AFM) images were taken by Cypher S microscopy (Oxford Instruments Plc., Oxford, UK). Transmission electron microscopy (TEM) and high-resolution transmission electron microscopy (HRTEM) images were obtained using a JEOL model JEM2100 instrument (JEOL Ltd., Tokyo, Japan) at an accelerating voltage of 200 kV. X-ray photoelectron spectroscopy (XPS) analysis (PHI5000 Versaprobe, Ulvac-Phi Inc. Kanagawa, Japan) was used to determine the chemical composition of the products. Raman spectra were obtained on a Raman spectrometer (JY T64000, HORIBA Jobin Yvon Inc., Paris, France) excited by the 514.5 nm line of an Ar^+ laser under 100 mW. UV-absorption behavior of samples was tested using a UV-3600 spectrophotometer (Shimadzu Corp., Kyoto, Japan).

3.3. Measurement

Photocatalytic measurements were carried out with a computer-controlled potentiostat (CHI660D) in a standard three-electrode cell using Ag/AgCl electrode as the reference electrode and a platinum wire as the counter electrode. WS_2 samples (9 mg), acetylene carbon (1 mg), and 2% polyvinylidene fluoride (PVDF) N-methyl-pyrrolidone (NMP) solution (150 μL) were mixed. The slurry was then coated onto ITO (Indium tin oxide) conductive glass (1 cm × 1 cm) and dried to form a thin-film electrode, used as the working electrode. Linear sweep voltamperometry was performed in 0.5 M Na_2SO_4 solution with a scan rate of 10 mV/s. A 500 W Xe lamp served as the light source in the photoelectrochemical measurements.

4. Conclusions

We used a facile sonication preparation of WS_2 quantum dots from hydrothermal synthesized WS_2 powders. A sulfuration process was applied to reduce defects and improve the electrical properties of WS_2. Uniform WS_2 QDs with an average size of ~3 nm exhibited unique optical and electrical properties. The abundant active edge sites of QDs led to good photocatalytic activity for hydrogen evolution. The current density of WS_2 QDs under illumination was raised almost two times higher than that of the pristine WS_2. Our results may provide an effective approach to synthesize and modify TMDC QDs, and demonstrate the promising photocatalytic application of TMDC QD materials.

Acknowledgments: This work was financially supported by the National Basic Research Program of China (973 Program: 2013CB932903), the National Science Foundations of China (No. 61205057, No. 11574136), the Qing Lan Project, the "1311 Talent Plan" Foundation of Nanjing University of Posts and Telecommunications, the Six Talent Peaks Project in Jiangsu Province (JY-014), and Jiangsu Provincial Key R & D Program (Grant No. BE2015700).

Conflicts of Interest: The authors declare no competing financial interest.

References

1. Deng, D.; Novoselov, K.S.; Fu, Q.; Zheng, N.; Tian, Z.; Bao, X. Catalysis with two-dimensional materials and their heterostructures. *Nat. Nanotechnol.* **2016**, *11*, 218–230. [CrossRef] [PubMed]
2. Chhowalla, M.; Shin, H.S.; Eda, G.; Li, L.J.; Loh, K.P.; Zhang, H. The chemistry of two-dimensional layered transition metal dichalcogenide nanosheets. *Nat. Chem.* **2013**, *5*, 263–275. [CrossRef] [PubMed]
3. Tian, H.; Chin, M.L.; Najmaei, S.; Guo, Q.; Xia, F.; Wang, H.; Dubey, M. Optoelectronic devices based on two-dimensional transition metal dichalcogenides. *Nano Res.* **2016**, *9*, 1543–1560. [CrossRef]
4. Voiry, D.; Salehi, M.; Silva, R.; Fujita, T.; Chen, M.; Asefa, T.; Chhowalla, M. Conducting MoS_2 nanosheets as catalysts for hydrogen evolution reaction. *Nano Lett.* **2013**, *13*, 6222–6227. [CrossRef] [PubMed]
5. Chu, D.; Zhang, C.; Yang, P.; Du, Y.; Lu, C. WS_2 as an Effective Noble-Metal Free Cocatalyst Modified $TiSi_2$ for Enhanced Photocatalytic Hydrogen Evolution under Visible Light Irradiation. *Catalysts* **2016**, *6*, 136. [CrossRef]
6. Xiang, Q.J.; Yu, J.G.; Jaroniec, M. Synergetic Effect of MoS_2 and Graphene as Cocatalysts for Enhanced Photocatalytic H_2 Production Activity of TiO_2 Nanoparticles. *J. Am. Chem. Soc.* **2012**, *134*, 6575–6578. [CrossRef] [PubMed]
7. Adriano, A.; Zdenêk, S.; Martin, P. 2H-1T phase transition and hydrogen evolution activity of MoS_2, $MoSe_2$, WS_2 and WSe_2 strongly depends on the MX_2 composition. *Chem. Commun.* **2015**, *51*, 8450–8453.
8. Shi, J.; Tong, R.; Zhou, X.; Gong, Y.; Zhang, Z.; Ji, Q.; Liu, Z. Temperature-Mediated Selective Growth of MoS_2/WS_2 and WS_2/MoS_2 Vertical Stacks on Au Foils for Direct Photocatalytic Applications. *Adv. Mater.* **2016**, *28*, 10664–10672. [CrossRef] [PubMed]
9. Yang, J.; Voiry, D.; Ahn, S.J.; Kang, D.; Kim, A.Y.; Chhowalla, M.; Shin, H.S. Two-Dimensional Hybrid Nanosheets of Tungsten Disulfide and Reduced Graphene Oxide as Catalysts for Enhanced Hydrogen Evolution. *Angew. Chem. Int. Ed.* **2013**, *52*, 13751–13754. [CrossRef] [PubMed]
10. Xie, J.; Zhang, H.; Li, S.; Wang, R.; Sun, X.; Zhou, M.; Zhou, J.; Lou, X.W.; Xie, Y. Defect-Rich MoS_2 Ultrathin Nanosheets with Additional Active Edge Sites for Enhanced Electrocatalytic Hydrogen Evolution. *Adv. Mater.* **2013**, *25*, 5807–5813. [CrossRef] [PubMed]
11. Voiry, D.; Yamaguchi, H.; Li, J.; Silva, R.; Alves, D.C.; Fujita, T.; Chhowalla, M. Enhanced catalytic activity in strained chemically exfoliated WS_2 nanosheets for hydrogen evolution. *Nat. Mater.* **2013**, *12*, 850–855. [CrossRef] [PubMed]
12. Backes, C.; Szydłowska, B.M.; Harvey, A.; Yuan, S.; Vega-Mayoral, V.; Davies, B.R.; Blau, W.J. Production of Highly Monolayer Enriched Dispersions of Liquid-Exfoliated Nanosheets by Liquid Cascade Centrifugation. *ACS Nano* **2016**, *10*, 1589–1601. [CrossRef] [PubMed]
13. Nguyen, T.P.; Sohn, W.; Oh, J.H.; Jang, H.W.; Kim, S.Y. Size-Dependent Properties of Two-Dimensional MoS_2 and WS_2. *J. Phys. Chem. C* **2016**, *120*, 10078–10085. [CrossRef]
14. Zhang, X.; Lai, Z.; Liu, Z.; Tan, C.; Huang, Y.; Li, B.; Zhang, H. A Facile and Universal Top-Down Method for Preparation of Monodisperse Transition-Metal Dichalcogenide Nanodots. *Angew. Chem. Int. Ed.* **2015**, *54*, 5425–5428. [CrossRef] [PubMed]
15. Gopalakrishnan, D.; Damien, D.; Shaijumon, M.M. MoS_2 Quantum Dot-Interspersed Exfoliated MoS_2 Nanosheets. *ACS Nano* **2014**, *8*, 5297–5303. [CrossRef] [PubMed]
16. Liu, D.; Guo, Y.; Fang, L.; Robertson, J. Sulfur vacancies in monolayer MoS_2 and its electrical contacts. *Appl. Phys. Lett.* **2013**, *103*, 183113. [CrossRef]
17. Wei, J.W.; Ma, Z.W.; Zeng, H.; Wang, Z.Y.; Wei, Q.; Peng, P. Electronic and optical properties of vacancy-doped WS_2 monolayers. *AIP Adv.* **2012**, *2*, 042141. [CrossRef]
18. Makarova, M.; Okawa, Y.; Aono, M. Selective adsorption of thiol molecules at sulfur vacancies on MoS_2 (0001), followed by vacancy repair via S–C dissociation. *J. Phys. Chem. C* **2012**, *116*, 22411–22416. [CrossRef]
19. Yu, Z.; Pan, Y.; Shen, Y.; Wang, Z.; Ong, Z.Y.; Xu, T.; Wang, J. Towards intrinsic charge transport in monolayer molybdenum disulfide by defect and interface engineering. *Nat. Commun.* **2014**, *5*. [CrossRef] [PubMed]

20. Zhou, L.; Yan, S.; Pan, L.; Wang, X.; Wang, Y.; Shi, Y. A scalable sulfuration of WS_2 to improve cyclability and capability of lithium-ion batteries. *Nano Res.* **2016**, *9*, 857–865. [CrossRef]
21. Zhao, X.; Ma, X.; Sun, J.; Li, D.H.; Yang, X.R. Enhanced Catalytic Activities of Surfactant-Assisted Exfoliated WS_2 Nanodots for Hydrogen Evolution. *ACS Nano* **2016**, *10*, 2159–2166. [CrossRef] [PubMed]
22. Morrish, R.; Haak, T.; Wolden, C.A. Low-temperature synthesis of *n*-type WS_2 thin films via H_2S plasma sulfurization of WO_3. *Chem. Mater.* **2014**, *26*, 3986–3992. [CrossRef]
23. Liang, L.; Meunier, V. First-principles Raman spectra of MoS_2, WS_2 and their heterostructures. *Nanoscale* **2014**, *6*, 5394–5401. [CrossRef] [PubMed]
24. Zhao, W.; Ghorannevis, Z.; Amara, K.K.; Pang, J.R.; Toh, M.; Zhang, X.; Eda, G. Lattice dynamics in mono-and few-layer sheets of WS_2 and WSe_2. *Nanoscale* **2013**, *5*, 9677–9683. [CrossRef] [PubMed]
25. Berkdemir, A.; Gutiérrez, H.R.; Botello-Méndez, A.R.; Perea-López, N.; Elías, A.L.; Chia, C.I.; Terrones, H. Identification of individual and few layers of WS_2 using Raman Spectroscopy. *Sci. Rep.* **2013**, *3*. [CrossRef]
26. Xu, S.J.; Li, D.; Wu, P.Y. One-Pot, Facile, and Versatile Synthesis of Monolayer MoS_2/WS_2 Quantum Dots as Bioimaging Probes and Effi cient Electrocatalysts for Hydrogen Evolution Reaction. *Adv. Funct. Mater.* **2015**, *25*, 1127–1136. [CrossRef]
27. Lin, L.; Xu, Y.; Zhang, S.; Ross, I.M.; Ong, A.C.; Allwood, D.A. Fabrication of luminescent monolayered tungsten dichalcogenides quantum dots with giant spin-valley coupling. *ACS Nano* **2013**, *7*, 8214–8223. [CrossRef] [PubMed]
28. Wang, T.; Liu, L.; Zhu, Z.; Papakonstantinou, P.; Hu, J.; Liu, H.; Li, M. Enhanced electrocatalytic activity for hydrogen evolution reaction from self-assembled monodispersed molybdenum sulfide nanoparticles on an Au electrode. *Energ. Environ. Sci.* **2013**, *6*, 625–633. [CrossRef]
29. Sun, Y.; Sun, Z.; Gao, S.; Cheng, H.; Liu, Q.; Lei, F.; Xie, Y. All-Surface-Atomic-Metal Chalcogenide Sheets for High-Efficiency Visible-Light Photoelectrochemical Water Splitting. *Adv. Energy Mater.* **2014**, *4*, 1300611. [CrossRef]